JOURNAL OF SPACECRAFT AND ROCKETS
Vol. 33, No. 5, September–October 1996

Numerical Study of Low-Thrust Nozzles for Satellites

S. M. Liang,* K. L. Huang,† and K. C. Chen†
National Cheng Kung University, Tainan 701, Taiwan, Republic of China

Axisymmetric low-thrust nozzles were numerically investigated for their performance. Both the Euler and Navier–Stokes solvers were developed for studying the flowfields and the viscous effect of the nozzle flows. The low-thrust nozzles considered are the conventional conical nozzle and the minimum-length nozzle. These two types of nozzle were analyzed and compared for their performance by varying the values of geometric parameters and were designed to produce short nozzles with a required thrust for satellite control. Since a minimum-length nozzle may be too long, causing an additional energy loss in the boundary layer, and too heavy for economic considerations, a technique of cutting off the supersonic section about 71% at a distance 10 throat radii from the throat is suggested, with only a 2% loss in the thrust and specific impulse ratios for the viscous model. The losses can be compensated by increasing the throat area by the same percentage. It was also found that the lower the wall temperature, the greater the mass flow rate needed to maintain the required thrust. Consequently, a low wall temperature will reduce the nozzle efficiency.

Nomenclature

A = cross-sectional area
C_d = mass flow coefficient ($=\dot{m}/\dot{m}_i$)
CFL = Courant number
c = speed of sound
F = thrust
I_{sp} = specific impulse ($=F/\dot{m}$)
$\dot{m}$ = mass flow rate
R_c = inlet radius of curvature
R_{ci} = throat radius of curvature
Re = Reynolds number based on the throat radius of the nozzle
R_{th} = throat radius
T = temperature
x, y = dimensionless Cartesian coordinates unless otherwise noted
γ = specific heat ratio
θ = half angle of divergence
ρ = density
ϕ = half angle of convergence

Subscripts

i = isentropic condition
i, j = grid indices
t = stagnation condition
th = nozzle throat

Introduction

THRUSTERS in a satellite provide controlled impulse for orienting the satellite spin axes during spinning phases; adjusting the orbit; controlling the attitude, the spin rate, and the nutation; and providing three-axis attitude control for the satellite in conjunction with the attitude controlled system. In general, a satellite contains a number of thrusters, typically more than 12. Thrusters can be categorized into high and low thrusters. High thrusters are used for orbit changes and low thrusters for orbit adjustment, orientation, etc. The thrust range of low thrusters is usually from 0.2 to 100 lb. This study focuses on the design of short-length nozzles used for low-thrust thrusters by numerical simulation.

In the past several decades, many researchers have studied nozzle performance. A simple method is the method of characteristics (MOC). For example, Rao[1] used the MOC to design a short nozzle with a wall contour that yields optimal thrust. To optimize the nozzle length, a class of MOCs was used to design a nozzle with a minimum throat-to-exit length and a uniform exit flow. Such nozzles are called minimum-length nozzles (MLNs). Note that an MLN, which is essentially a supersonic nozzle, is not necessarily a short nozzle. Moreover, the distinctive feature of the class of MLNs is a sharp corner near the throat that connects the throat contour and the contoured nozzle wall. Most nozzles that are not MLNs have a smooth contoured wall at the throat.

There are two types of MLN.[2] One type assumes a straight sonic line at the throat, and the other a curved sonic line. Argraw and Emanuel[3] showed that the lengths of these two types of axisymmetric MLNs are almost the same.

In 1972 Cuffel et al.[4] investigated a supersonic conical nozzle and its performance. Kushida et al.[5] studied the performance of a high-area-ratio nozzle in comparison with experimental data. In numerical simulation, Chang et al.[6] simulated supersonic viscous flows in high-expansion-ratio rocket nozzles. Zha and Bilgen[7] studied the effect of throat contouring of a nonaxisymmetric nozzle by using the upwind relaxation-sweeping algorithm to solve the three-dimensional Navier–Stokes equations. Bae and Emanuel[8] used an analytic method to investigate the performance of an aerospace plane propulsion nozzle. They found that there is little loss in the thrust when the upper nozzle wall is truncated. Korte et al.[9] combined a least-squares method and the parabolized Navier–Stokes solver to optimize hypersonic wind-tunnel nozzle contours.

In this study the performance of low-thrust nozzles was studied by using our Euler/Navier–Stokes solvers, which employed an improved implicit total-variation-diminishing scheme.[10] The nozzles were assumed to be operated in a vacuum environment, and the flow was underexpanded. The influence of the nozzle length on the nozzle performance was also investigated. The nozzle performance was represented by the performance parameters—the flow coefficient, the thrust, and the specific impulse ratios. Since the MLN may be too long and too heavy to install in satellites for economic reasons, a technique of cutting off part of the supersonic section of the nozzle was applied to shorten the length of MLNs.

Numerical Method

The governing equations of an axisymmetric nozzle flow are the compressible Reynolds-averaging Navier–Stokes equations associated with an algebraic turbulence model in Ref. 11. The equations were expressed in a strong conservation-law form and in a body-fitted coordinate system and were discretized using an implicit total-variation-diminishing scheme[12] in a finite volume fashion. The discretized equations were solved by using an ADI method[13] with a local time step. To enhance the convergence rate for a steady-state

Received Sept. 1, 1995; revision received Feb. 13, 1996; accepted for publication Feb. 20, 1996.

*Professor, Institute of Aeronautics and Astronautics. Member AIAA.
†Graduate Student, Institute of Aeronautics and Astronautics.

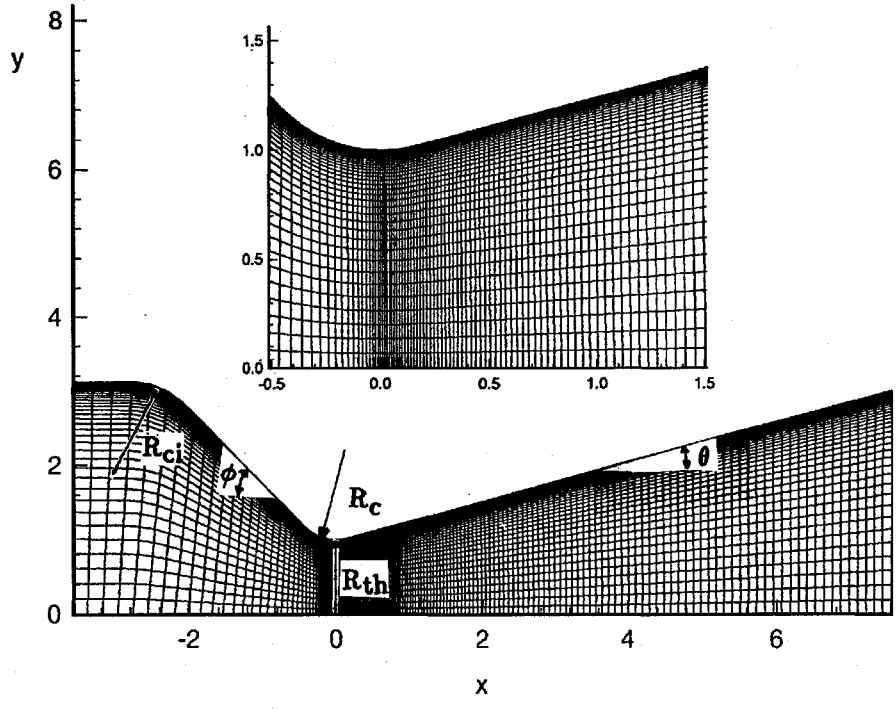

Fig. 1 170 × 40 grid used in the test problem.

solution, improved flux limiters suggested in Ref. 10 were used. For example, the flux limiter at a cell interface $(i + \frac{1}{2}, j)$ is of the form

$$g_{i+\frac{1}{2},j} = \text{minmod}\left(\alpha_{i-\frac{3}{2},j}, \alpha_{i-\frac{1}{2},j}, \alpha_{i+\frac{1}{2},j}\right)$$

Here, α denotes the characteristic variable. The function minmod of two or more arguments is equal to the smallest number in absolute value if all the arguments are of the same sign and is equal to zero if any two arguments are of opposite sign. The flux limiter has the feature of more upwinding than for others in Ref. 10.

Boundary Conditions

At the inlet, the boundary condition specified is based on the one-dimensional characteristic theory. The number of boundary conditions specified depends on the number of characteristics along which the signal propagates from the interior to the boundary. On the nozzle wall, the tangency condition is imposed for the inviscid model and the no-slip condition for the viscous model. For most of the calculations, the wall is assumed to be adiabatic; exceptions are particularly mentioned. On the nozzle wall, the density is extrapolated from interior points and the pressure is found from the normal momentum equation. When the nozzle wall is kept at a constant temperature, the density is calculated from the equation of state and the pressure obtained from the normal momentum equation. The boundary condition at the symmetric axis is the symmetry condition. Thus, two fictitious grid cells outside the symmetric axis are used. On the symmetric axis, a second-order extrapolation method[14] is employed to obtain the values of the flow variables. Since the ambient pressure is assumed to be zero, the nozzle flows are underexpanded. The flow quantities at the exit plane are extrapolated from the upstream points, since most of the exit region is supersonic. Although other boundary conditions in the subsonic boundary layer at the exit were not investigated, Chang et al.[6] have shown that the extrapolation condition is normally able to produce reasonable results for viscous supersonic nozzle flows.

Grid Generation

The grids used for this study are generated by the Poisson equations, which control the grid stretching through the source terms.[15]

Results and Discussion

Code Validation

To validate the accuracy of the present axisymmetric Euler/Navier–Stokes solver, the conical supersonic nozzle studied in Ref. 16 is tested. The nozzle contour associated with a grid with

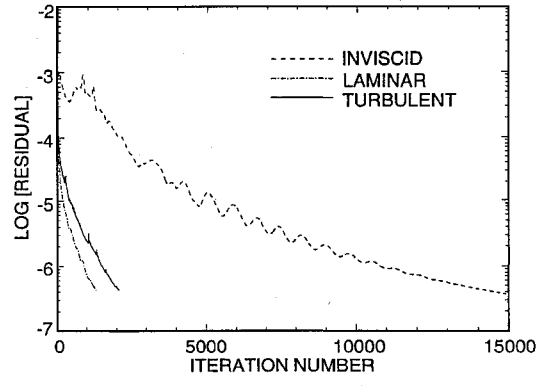

Fig. 2 Convergence histories for the inviscid, laminar, and turbulent flow models.

170 × 40 grid points is shown in Fig. 1. A subplot for x between −0.5 and 1.5 is also included to see the extent of grid clustering near the throat ($x = 0$), because a fast flow expansion occurs there. Note that the coordinates (x, y) are dimensionless; they have been normalized by the characteristic length, the nozzle throat radius. Other grids with 140 × 30 and 170 × 50 points were also tried. The improvements in the nozzle performance using more grid points were found to be very small. Thus the 140 × 40 grid is used. The geometric data on the nozzle are the half angle of convergence, $\phi = 45$ deg; the half angle of divergence, $\theta = 15$ deg; and the area ratios at the inlet and the exit, $A_{\text{inlet}}/A_{\text{th}} = 9.76$ and $A_{\text{exit}}/A_{\text{th}} = 9$, respectively. Moreover, the ratio of the contraction radius of curvature to the throat radius is set at $R_{\text{ci}}/R_{\text{th}} = 1$, and the ratio of the throat radius of curvature to the throat radius at $R_c/R_{\text{th}} = 0.625$. The working fluid is air with specific heat ratio $\gamma = 1.4$. With these values of the exit area ratio and γ, the isentropic exit Mach number is 3.806. The total pressure and the total temperature are, respectively, 70 psia and 540°R, as used in the experiment.[4] The Reynolds number is chosen to be 1.8×10^6, and CFL is chosen to be 2.

The convergence histories are shown in Fig. 2. Note that the inviscid flow solution is used as an initial guess for the viscous flow solutions. So the viscous flow calculations take fewer iterations than for the inviscid model. The computed Mach-number and pressure distributions along the wall and the centerline are shown in Fig. 3. The experimental data[4] are included for comparison. The present results are in good agreement with the experimental data except for a small difference in the vicinity of $x = 0.25$. Note that the

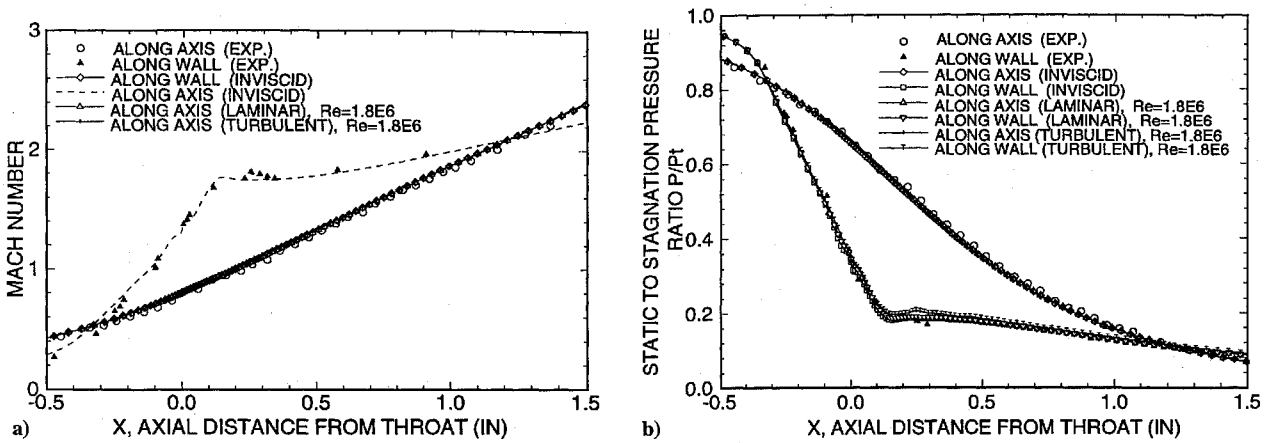

Fig. 3 Comparison of the computed a) Mach-number and b) pressure distributions along the centerline and the wall with the experimental data.

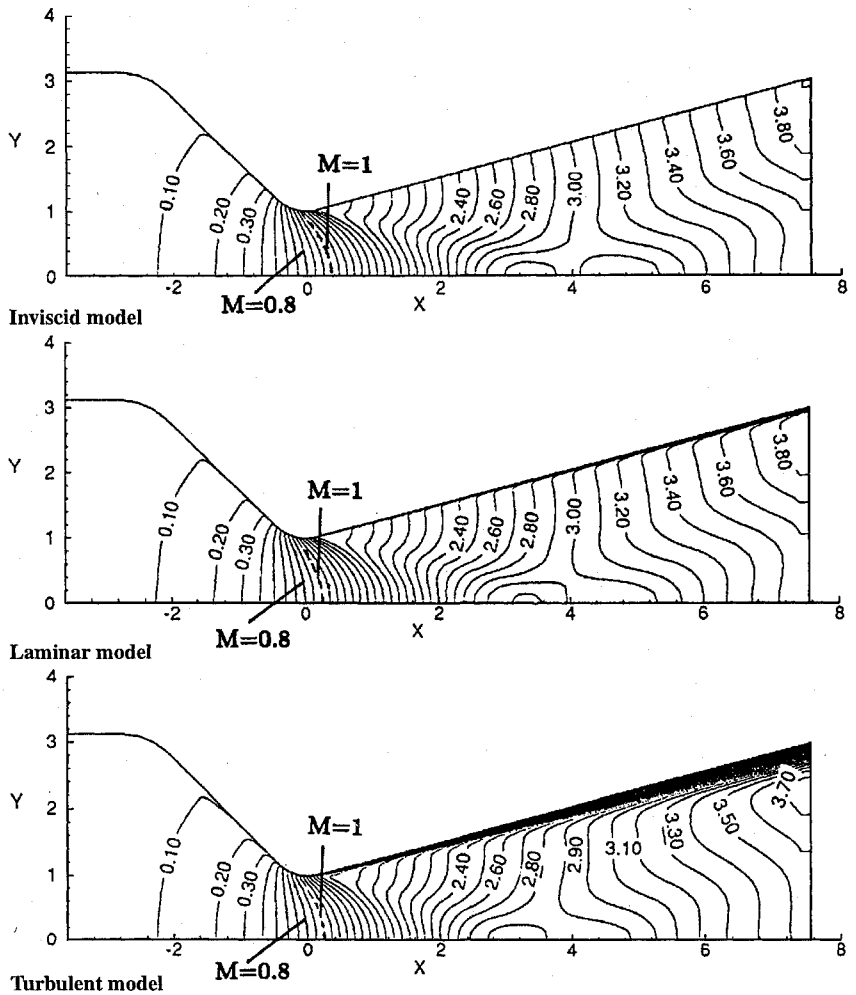

Fig. 4 Mach-number contours.

turbulent and laminar solutions are hard to distinguish. In the vicinity of $x = 0.25$, the turbulent solutions are slightly overpredicted in comparison with the experimental data. The Mach-number contours obtained by the inviscid, turbulent, and laminar models are shown in Fig. 4. From the Mach-number contours, the curved sonic line near the throat is clearly seen, and an oblique shock wave with its reflection from the centerline is visible, although the shock wave has been smeared out numerically. The oblique shock wave can be resolved by a fine grid or by using an unstructured adaptive grid technique.[17] The shock wave is estimated to originate from $x = 0.18$, which is close to the design juncture ($x = 0.14$) that connects the circular-arc throat and the straight nozzle wall. An interesting result is that the $M = 0.8$ contour that passes the throat location ($x = 0$) agrees well with the experimental result of Cuffel et al.[4]

Figure 4 also indicates that, at the Reynolds number of 1.8×10^6, the laminar solution is closer to the inviscid solution than to the turbulent solution. The reason is that the laminar flow has a smaller value of viscosity, resulting in a thinner boundary layer than that for the turbulent flow. At the exit plane, the Mach number in the core region is about 3.55 for the turbulent flow, which is slightly smaller than the Mach number of 3.59 for the laminar flow. This is because the laminar flow has a much thinner boundary layer to allow more expansion to be accomplished in the nozzle. Moreover, it was found that the turbulent flow has a larger core region with a uniform Mach number of 3.55 at the exit plane than the laminar flow has.

From these results, it is concluded that the present Euler/ Navier–Stokes solver is reasonably accurate. However, the CPU time used to obtain the converged solutions is pretty long on a computer work-

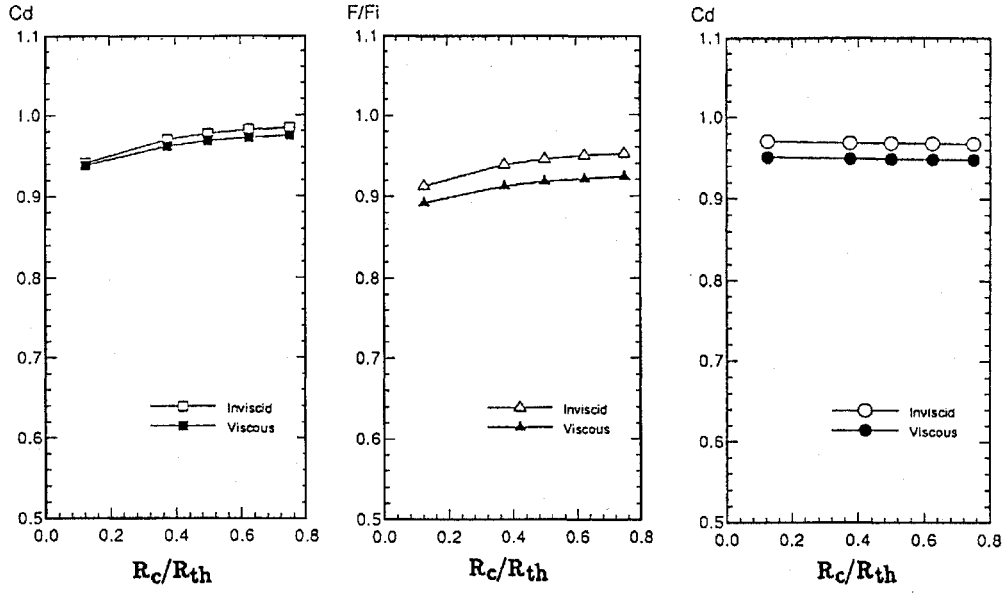

Fig. 5 Effect of the parameter R_c/R_{th} on nozzle performance.

station. It took about 15.5, 21.9, and 35.7 CPU hours for the inviscid, laminar, and turbulent flows on a DEC-alpha 3000 workstation.

Analysis and Design of Conventional Conical Nozzles

The conical nozzle in Ref. 16 is analyzed for nozzle performance by varying the values of the geometric parameters. The nozzle has area ratios of $A_{inlet}/A_{th} = 9.76$ and $A_{exit}/A_{th} = 9$. The ratio of specific heats is chosen to be 1.25. With the assumed values of the exit area and specific heat ratios, the isentropic Mach number is 3.343. The nozzle performance is evaluated from the values of the mass flow rate, the thrust, and the specific impulse, which will be normalized by the corresponding quantities at the one-dimensional isentropic condition. Let subscript i denote the isentropic condition. Thus we have the flow coefficient $\dot{m}/\dot{m}_i$, the thrust ratio F/F_i, and the specific impulse ratio I_{sp}/I_{spi}. In calculations of the thrust, the assumption of zero back pressure is used. Only the inviscid and turbulent models are considered. The Reynolds number is chosen to be 10^6, and CFL is chosen to be 2. The geometric parameters of the conical nozzle are R_{ci}/R_{th}, R_c/R_{th}, ϕ, and θ. The flowfields of different flow models and the effect of each parameter on the nozzle performance are investigated in the following.

First, the effect of the parameter R_{ci}/R_{th} on the nozzle performance is studied. The range of R_{ci}/R_{th} is 0.5 to 2. It was found that the influence of the inlet radius of curvature is not significant, and it can almost be neglected. Moreover, the flow viscosity can reduce the nozzle performance—about a 1% reduction on the flow coefficient, about a 3% reduction on the thrust ratio, and about a 2% reduction on the specific impulse ratio.

Figure 5 shows the effect of R_c/R_{th} on the nozzle performance. Unlike R_{ci}/R_{th}, the parameter R_c/R_{th} can affect the nozzle performance. The increases in C_d and F/F_i are about 3–4% for R_c/R_{th} varying from $\frac{1}{8}$ to $\frac{3}{4}$. This result explains that the smaller values of R_c/R_{th} induce a greater two-dimensional effect and consequently reduce the values of C_d and F/F_i. However, the variations of I_{sp}/I_{spi} with R_c/R_{th} are very small and can be neglected. This is because the variation of C_d is slightly larger than that for F/F_i as R_c/R_{th} increases.

The influence of the half angle of convergence is found to be not significant. The values of C_d and F/F_i are reduced very little (less than 1%), and the value of I_{sp}/I_{spi} is almost unchanged as ϕ varies from 30 to 85 deg. The loss percentages of C_d, F/F_i, and I_{sp}/I_{spi} due to the viscous effect are about 1, 3, and 2%, respectively.

Finally, the effect of the half angle of divergence is investigated. We found the effect of θ on C_d is within 1%, but the variation of θ induces an approximately 3% loss in the thrust ratio F/F_i and a 2% loss in the specific impulse ratio I_{sp}/I_{spi} as θ varies from 12 to 22 deg. This means that a larger half angle of divergence causes a larger radial component of momentum, which does not contribute to the axial-direction thrust. On the other hand, a smaller angle θ results in a longer nozzle, associated with more weight and energy loss caused by a longer boundary layer. Thus an optimal half angle of divergence will exist. The viscous effect in this case causes about a 3% loss for the thrust and specific impulse ratios but a negligible loss for the flow coefficient, because the convergent section and the throat shape are not changed.

Based on these results, it is concluded that the effective geometric parameters are R_c/R_{th} and θ but not R_{ci}/R_{th} and ϕ. By taking the factors of the viscous effect and the nozzle length into account, the optimal values of R_c/R_{th} and θ were found to be approximately 0.625 and 15 deg, respectively, by observing our computed data.

Analysis of MLNs

An MLN is a nozzle consisting of a subsonic convergent section and a supersonic section with a contoured shape designed by the method of characteristics. The nozzle has a sharp juncture that connects the circular-arc throat and the contoured nozzle wall. In this study, the values of the geometric parameters R_{ci}/R_{th}, R_c/R_{th}, and ϕ of the nozzle are chosen to be 1, 0.625, and 45 deg, respectively. The inlet and exit area ratios are chosen to be 9.76 and 40, respectively. The nozzle exit is located at $x = 35.45$. The value of γ is chosen to be 1.25. With these values of the exit area and specific heat ratios, the isentropic exit Mach number is 4.538. The corresponding dimensionless mass flow rate, thrust, and specific impulse are 0.59, 1.36, and 2.31, respectively. Note that the dimensional mass flow rate and thrust have been normalized by $\rho_t c_t A_{th}$ and $\rho_t c_t^2 A_{th}$, respectively, to obtain the corresponding dimensionless quantities, where subscript t denotes the upstream stagnation condition.

The sharp juncture in the nozzle was replaced by a small circular arc with the ratio of the radius of curvature to R_{th} equal to 0.02. A grid of 170 × 70 grid points, similar to Fig. 1, was used. The computed solutions obtained by the Euler and (turbulent) Navier–Stokes solvers are, respectively, shown in Figs. 6a and 6b. A curved, oblique shock wave with its reflection from the centerline in each figure and the curved sonic line in each subplot are clearly seen. Both solutions indicate that on the throat cross-sectional plane most of the region is subsonic. Moreover, the viscous effect that acts from the beginning of the contoured shape of the nozzle causes an upstream movement of the shock impingement point on the centerline because of the development of the boundary layer along the wall. But the flow viscosity does not have any effect on the upstream Mach-number contour before the throat, since the boundary layer developed is very thin. At the exit, the maximum Mach number is found to be 4.50

for the inviscid flow and 4.37 for the viscous flow. In both cases, the exit Mach numbers are lower than the isentropic exit Mach number. The reason is obvious: the inviscid flow has an energy loss due to the oblique shock wave, and the viscous flow has an energy loss due to the flow viscosity in addition to the shock wave. Moreover, the viscous case has a uniform core region with an exit Mach number of 4.32, whereas the inviscid case has a smaller core region and a slightly higher exit Mach number of 4.44.

To see the advantages and disadvantages of the MLN, the flow in a conical nozzle with the same exit area ratio as used in the MLN and $\theta = 15$ deg is computed. The conical nozzle has the exit location $x = 19.98$, shorter than for the MLN. Obviously, these two nozzles have different nozzle lengths but the same isentropic exit Mach number. It was found that the oblique shock waves predicted by the inviscid and viscous models have a large inclination angle with the axial flow. The performance of the two different-type nozzles is shown in Figs. 7 and 8 and tabulated at different x stations in Tables 1 and 2.

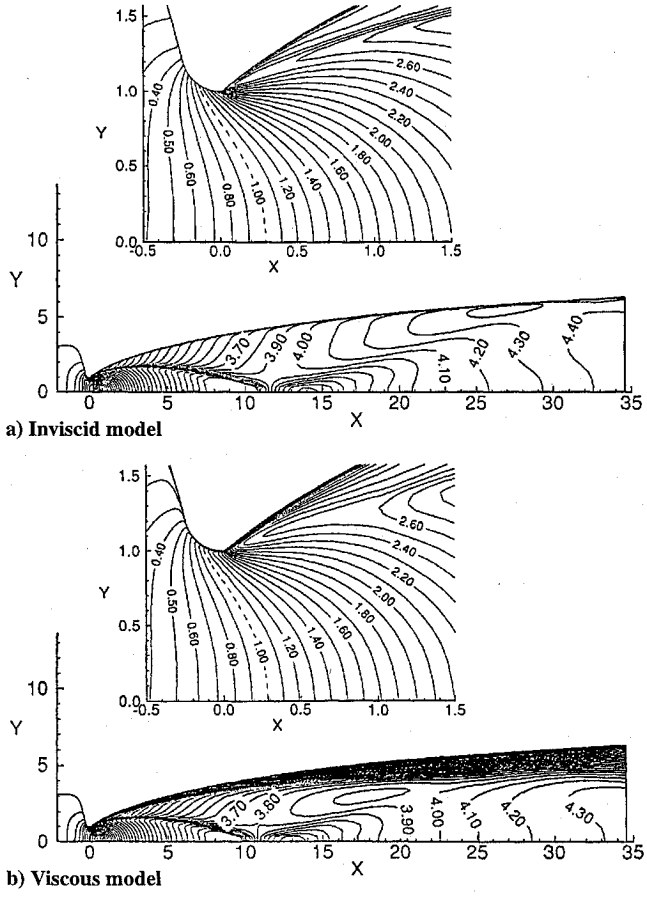

Fig. 6 Flowfields of Mach-number contours of the MLN.

From Fig. 7, one can see that the flow coefficients predicted by the inviscid and viscous models remain almost a constant as x (the exit location) varies from 0 (the throat location) to 34.53. The thrust and specific impulse ratios from the inviscid solution grow slowly for large values of x. However, the thrust and specific impulse ratios from the viscous solution become almost constant ($F/F_i = 0.87$–0.88, $I_{sp}/I_{spi} = 0.92$–0.93) for $x \geq 12.5$ (refer to Table 1). This constant value implies that the part of the supersonic section after $x = 12.5$ is redundant, because this section makes no significant contribution to the nozzle performance. The inviscid model predicts higher values for the thrust and specific impulse ratios than does the viscous model. The maximum deviation is about 6% for the thrust ratio and 7% for the specific impulse ratio.

Table 1 Performance of an MLN with different lengths

Exit position	Inviscid model		Viscous model	
x/R_{th}	F/F_i	I_{sp}/I_{spi}	F/F_i	I_{sp}/I_{spi}
5.0	0.8446	0.8884	0.8225	0.8702
7.5	0.8755	0.9228	0.8473	0.8992
10.0	0.8917	0.9420	0.8650	0.9135
12.5	0.9042	0.9539	0.8715	0.9205
15.0	0.9146	0.9617	0.8771	0.9244
17.5	0.9206	0.9672	0.8793	0.9265
20.0	0.9261	0.9710	0.8801	0.9277
34.53	0.9389	0.9844	0.8821	0.9289

Table 2 Performance of a conical nozzle with different lengths

Exit position	Inviscid model		Viscous model	
x/R_{th}	F/F_i	I_{sp}/I_{spi}	F/F_i	I_{sp}/I_{spi}
5.0	0.8322	0.8767	0.8142	0.8629
7.5	0.8642	0.9061	0.8428	0.8890
10.0	0.8863	0.9254	0.8638	0.9069
12.5	0.9041	0.9422	0.8804	0.9229
15.0	0.9176	0.9565	0.8919	0.9348
17.5	0.9270	0.9678	0.8998	0.9440
19.88	0.9312	0.9763	0.9017	0.9507

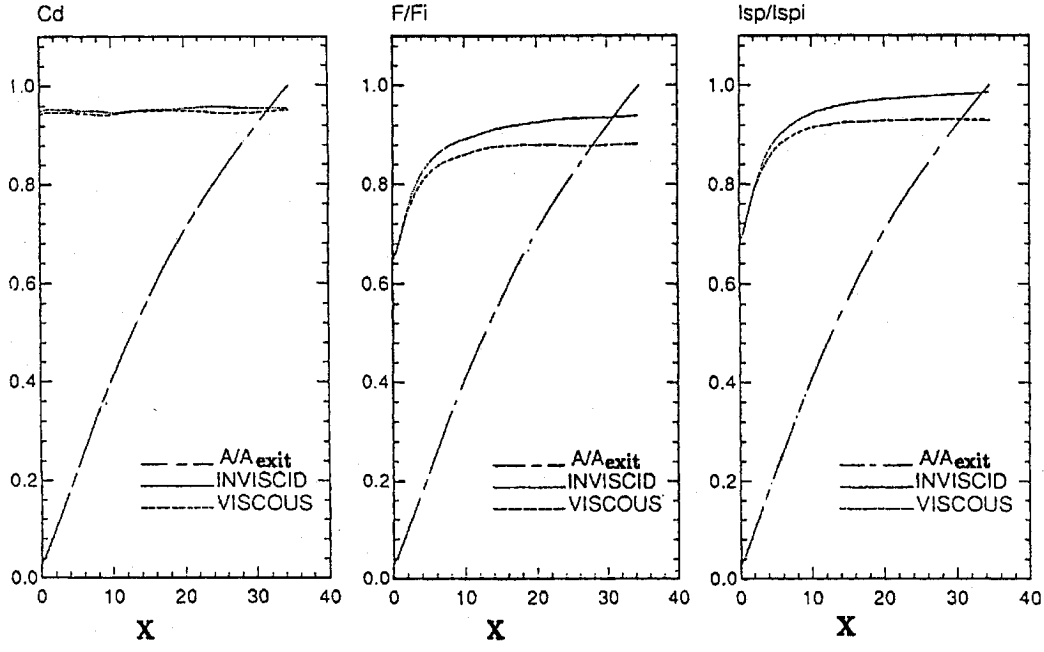

Fig. 7 Comparison of the performance of the MLN predicted by the inviscid and viscous models.

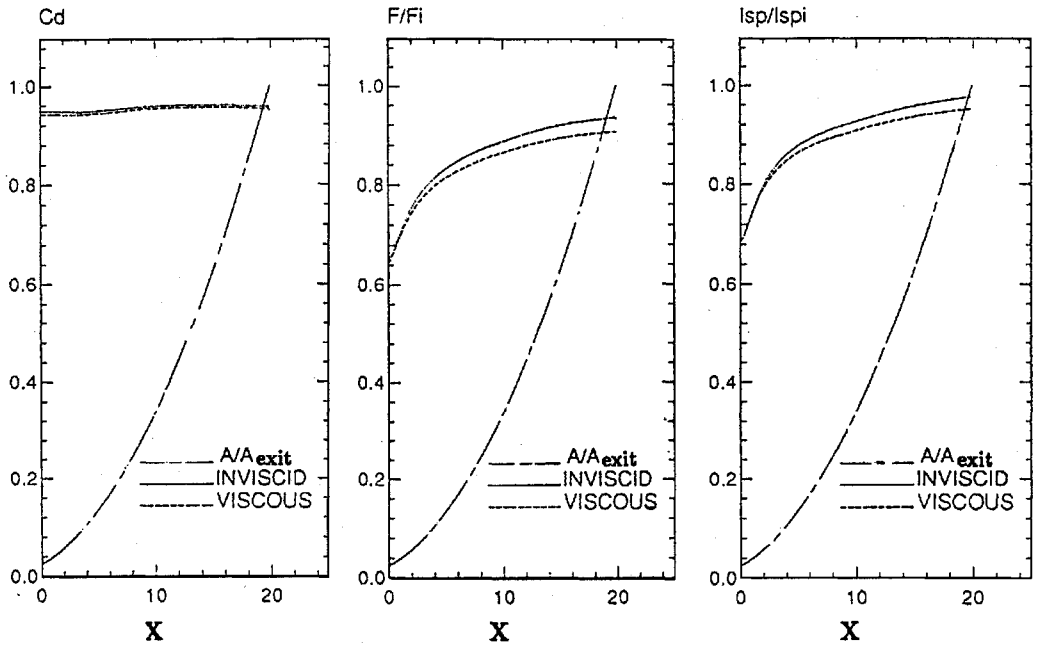

Fig. 8 Comparison of the performance of the conical nozzle predicted by the inviscid and viscous models.

The conical nozzle is found to perform as well as the MLN with regard to the predicted values of the performance parameters, as shown in Tables 1 and 2. As seen from Fig. 8, the increasing rates of F/F_i and I_{sp}/I_{spi} for larger values of x are greater than those for the MLN case, which are not constant over the range of x. Moreover, the viscous model predicts smaller values of F/F_i and I_{sp}/I_{spi}, at most about 3% lower than those for the inviscid model. Another interesting result is that for smaller values $x \leq 3$, the inviscid and viscous models predict the same results for the conical and minimum-length nozzles.

From economic considerations, a conventional unoptimized minimum-length nozzle may be too long and heavy for use in satellites. It was assumed that the nozzle is of uniform material. Thus, reducing the nozzle length results in a reduction in the nozzle weight. To reduce the nozzle length, we suggest cutting off the downstream nozzle about 71% from $x = 10$ to the exit, thus causing only a 2% loss in the thrust and specific impulse ratios for the viscous model and a 5% loss for the inviscid model. These losses can be compensated by increasing the throat area by the same percentages to allow more flow to reach the same performance level as the original nozzle. This conclusion was confirmed by calculating the suggested shorter MLN flow to check its performance; the comparison with the original MLN was satisfactory.

Effect of Wall Temperature

In these calculations, the results are based on the assumption of an adiabatic wall condition. The wall temperature may affect the nozzle performance. The nozzle in the test problem is now considered. The Reynolds number is chosen to be 1×10^6. Figure 9 shows the (cooling) effect of the wall temperature ratio (T_{wall}/T_t) on the nozzle performance. The thrust ratio is almost unchanged for T_{wall}/T_t between 0.1 and 0.7. As T_{wall}/T_t decreases from 0.7 to 0.1, the flow-coefficient ratio increases, but the specific impulse ratio decreases. The reason is that a lower wall temperature inhibits the boundary-layer growth, resulting in a thinner boundary layer and a flow-speed increase in the boundary layer. Moreover, we found that a low wall temperature has another effect on the density variation in the boundary layer. Namely, a cold wall was found to have much more influence on the density variation in the boundary layer before and near the throat than on the flow speed. Therefore, when $T_{wall}/T_t = 0.1$, the low wall temperature results in a greater increase in the mass flow rate than in other cases. In this case, it was found that the values of the dimensionless density near the wall at the throat can be as large as 2.5, which is larger than those values (about 0.6) in the case of $T_{wall}/T_t = 0.7$. From Fig. 9, it is clear that

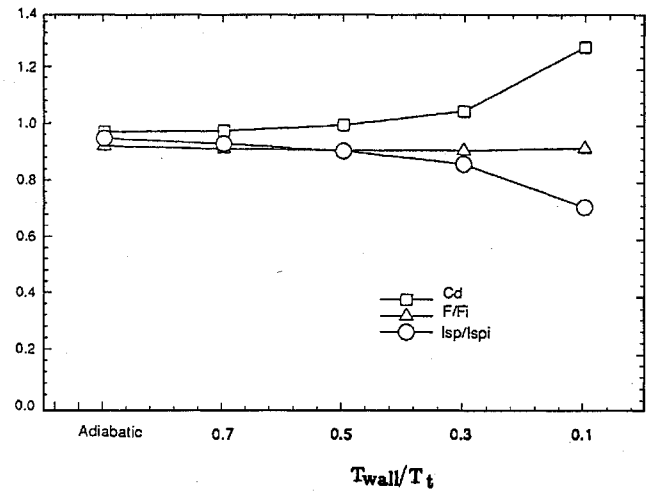

Fig. 9 Effect of the wall temperature on the nozzle performance.

when $T_{wall}/T_t = 0.5$–0.7 the nozzle performance is as good as the adiabatic wall case. When T_{wall}/T_t is less than 0.5, the nozzle efficiency is reduced, since the mass flow rate is significantly increased but not the thrust.

Conclusions

A reasonably accurate Euler/Navier–Stokes solver has been developed for analyzing the conventional conical nozzle and the MLN. The solver is based on the implicit total-variation-diminishing scheme with an improved flux limiter. From the present study we draw the following three conclusions:

1) For the conical nozzles the effective geometric parameters are the ratio of the throat radius of curvature to the throat radius and the half angle of divergence of the nozzle. The throat radius of curvature primarily affects the mass flow rate and the half angle of divergence for the thrust. The optimal values of R_c/R_{th} and θ are found to be 0.625 and 15 deg, respectively, by a careful examination of the computed data.

2) For the conventional MLNs designed by the method of characteristics, the use of MLNs is limited by the nozzle length. A longer MLN is associated with a thicker boundary layer. To reduce the nozzle length, an appropriate treatment can be made by cutting off a 71% length of the supersonic section of the nozzle at $x = 10$, a distance of $10R_{th}$ from the throat, although there is a 2% loss in the thrust ratio. This small loss can be compensated by increasing the

throat area to allow more flow, to reach the same performance level as the original nozzle.

3) When the wall temperature ratio T_{wall}/T_t ranges from 0.5 to 0.7, the predicted nozzle performance agrees with that for the corresponding nozzle with an adiabatic wall. It was found that the lower the wall temperature, the greater the mass flow rate that was needed for maintaining the same thrust level but with a lower nozzle efficiency. The reason is that a cold wall can result in a thinner boundary layer and an increase in the flow speed as well as a great increase in the density in the boundary layer, in particular, before and near the throat.

Acknowledgment

Support for this study under Contract NSC 82-F-SP-006-05 of the National Science Council is gratefully acknowledged.

References

[1]Rao, G. V. R., "Exhaust Nozzle Contour for Optimum Thrust," *Jet Propulsion*, Vol. 28, No. 6, 1958, pp. 377–382.

[2]Emanuel, G., *Gasdynamics: Theory and Applications*, AIAA Education Series, AIAA, New York, 1986, p. 307.

[3]Argraw, B. M., and Emanuel, G., "Comparison of Minimum Length Nozzles," *Journal of Fluids Engineering*, Vol. 1100, Sept. 1988, pp. 283–288.

[4]Cuffel, R. F., Back, L. H., and Massier, P. F., "Transonic Flowfield in a Supersonic Nozzle with Small Throat Radius of Curvature," *AIAA Journal*, Vol. 7, No. 7, 1969, pp. 1364–1366.

[5]Kushida, R. Hermel, J., Apfel, S., and Zydowicz, M., "Performance of High-Area-Ratio Nozzle for a Small Rocket Thruster," *Journal of Propulsion and Power*, Vol. 3, No. 4, 1987, pp. 329–333.

[6]Chang, C. L., Kronzon, Y., and Merkle, C. L., "Time-Iterative Solutions of Viscous Supersonic Nozzle Flows," *AIAA Journal*, Vol. 26, No. 10, 1988, pp. 1208–1215.

[7]Zha, G. C., and Bilgen, E., "Effect of Throat Contouring on Two Dimensional Convergent–Divergent Nozzle Using URS Method," AIAA Paper 92-2659, March 1992.

[8]Bae, Y. Y., and Emanuel, G., "Performance of an Aerospace Plane Propulsion Nozzle," *Journal of Aircraft*, Vol. 28, No. 2, 1991, pp. 113–122.

[9]Korte, J. J., Kumar, A., Singh, D. J., and B. Grossman, B., "Least-Squares/Parabolized Navier–Stokes Procedure for Optimizing Hypersonic Wind-Tunnel Nozzles," *Journal of Propulsion and Power*, Vol. 8, No. 5, 1992, pp. 1057–1063.

[10]Liang, S. M., Tsai, C. J., and Wu, R. N., "Efficient, Robust Second-Order Total Variation Diminishing Scheme," *AIAA Journal*, Vol. 34, No. 1, 1996, pp. 193–195.

[11]Baldwin, B. S., and Lomax, H., "Thin Layer Approximation and Algebraic Method for Separated Turbulent Flows," AIAA Paper 78-257, Jan. 1978.

[12]Yee, H. C., and Harten, A., "Implicit TVD Schemes for Hyperbolic Conservation Law in Curvilinear Coordinates," *AIAA Journal*, Vol. 25, No. 2, 1987, pp. 266–274.

[13]Beam, R. M., and Warming, R. F., "An Implicit Factored Scheme for the Compressible Navier–Stokes Equations," *AIAA Journal*, Vol. 16, No. 4, 1978, pp. 393–402.

[14]Harten, A., and Osher, S., "Uniformly High-Order Accurate Non-Oscillatory Schemes I," *SIAM Journal on Numerical Analysis*, Vol. 24, No. 2, 1987, pp. 279–309.

[15]Sorenson, R. L., "A Computer Program to Generate Two-Dimensional Grid About Airfoils and Other Shape by the Use of Poisson's Equations," NASA TM-81198, May 1980.

[16]Back, L. H., Massier, P. F., and Gier, H. L., "Comparison of Measured and Predicted Flows Through Conical Supersonic Nozzle, with Emphasis on the Transonic Region," *AIAA Journal*, Vol. 3, No. 9, 1965, pp. 1606–1613.

[17]Loth, E., Baum, J., and Lohner, R., "Formation of Shocks Within Axisymmetric Nozzles," *AIAA Journal*, Vol. 30, No. 1, 1992, pp. 268–270.

T. C. Lin
Associate Editor